Available online at www.sciencedirect.com

ScienceDirect

Advances in Space Research 77 (2026) 7054–7066

ADVANCES IN SPACE RESEARCH (a COSPAR publication)

www.elsevier.com/locate/asr

Space capacity-based metric to rank in orbit collision risk

Andrea Muciaccia [a,*], Francesca Letizia [c], Mirko Trisolini [b], Lorenzo Giudici [a], Stijn Lemmens [c], Juan Luis Gonzalo [d], Camilla Colombo [a]

[a] Department of Aerospace Science and Technology, Politecnico di Milano, Via La Masa 34, Milan 20156, Italy
[b] Vyoma GmbH, Karl-Theodor-Straße 55, Munich 80803, Germany
[c] European Space Agency (ESA), Keplerlaan 1, Noordwijk 2201 AZ, the Netherlands
[d] Aerospace Systems and Transport Research Group, Universidad Rey Juan Carlos, Av. del Alcalde de Mostoles, Mostoles, Madrid 28933, Spain

Received 18 July 2025; received in revised form 21 December 2025; accepted 23 January 2026
Available online 28 January 2026

Abstract

Space capacity is a developing concept, with new models to describe and quantify it emerging in recent years. These models aim to define a sustainable threshold for the space environment, a limit which ensures the continued safety of future launches and satellite operations. They also seek to link this threshold to the impact of both new and existing objects in orbit, effectively assigning each object a share of the total capacity, or the portion it consumes. This definition should be internationally recognised and adopted, serving as the foundation for launch guidelines, debris mitigation strategies, and, more broadly, global Space Traffic Management.

Within this work, the concept of space capacity refers to the capacity consumed by a population, examining how this consumption changes over time. The capacity model is applied to assess the level of risk posed by potential orbital fragmentation. The model compares the difference in space capacity consumption between a scenario with fragmentation and one without, in order to determine whether such an event has a significant impact on overall consumption. This approach provides more insights than just counting the number of objects or fragmentation events.

Keywords: Space capacity; In orbit fragmentations; Space debris; Space sustainability

1. Introduction

Since the beginning of the space age, the number of artificial objects in orbit has steadily increased (ESA Space Debris Office, 2024), with a notable increase in recent years driven by the rise of new satellite-based services. However, this has also led to an increase in collision or explosion events that involve the generation of new debris. Despite the guidelines for space debris mitigation and collision avoidance, some events are difficult to predict (e.g., collision between objects) or even unpredictable (e.g., explosion of a rocket body). The increase in the space debris population is a significant concern, as it exposes regions of space to a higher risk, potentially triggering fragmentation chain reactions (Kessler and Cour-Palais, 1978).

Consequently, it is essential to assess and quantify the impact (and the associated risk) of a new fragmentation event over both short-term and long-term timescales. The impact should be assessed not only with respect to the amount of debris added to the environment but also how long they will remain there and how they will interact with objects already in orbit. In this view, the method proposed in this work, involving the concept of space capacity, tries

* Corresponding author.
E-mail addresses: andrea.muciaccia@polimi.it (A. Muciaccia), francesca.letizia@esa.int (F. Letizia), mirko.trisolini@vyoma.space (M. Trisolini), lorenzo.giudici@polimi.it (L. Giudici), stijn.lemmens@esa.int (S. Lemmens), juan.gonzalo@urjc.es (J.L. Gonzalo), camilla.colombo@polimi.it (C. Colombo).

https://doi.org/10.1016/j.asr.2026.01.077
0273-1177/

to consider the problem from a different perspective. To quantify the risk level of fragmentation, one must start from the consideration that each fragmentation event has several characteristics. The type of event (i.e., collision, explosion), the number of objects involved and their mass are closely related to the number of fragments generated (as modelled in the NASA Standard Satellite Breakup Model Johnson et al. (2001)). An example is presented in Fig. 1, which compares the temporal evolution of the number of objects (greater than 1 cm in size) generated by an explosion and a catastrophic collision. For this example, the fragmentation was simulated in the same location and considering the same total mass; the main features are reported in Table 1.

The location of the fragmentation event, such as its altitude and inclination, and the orbital geometry play a critical role in determining both the likelihood of interaction with densely populated orbital regions and the nature of orbital perturbations acting on the resulting fragments. These factors influence the short- and long-term evolution of the debris. As illustrated in Fig. 2, two breakup events of the same type simulated at different altitudes shows this effect: the event occurring at the lower altitude (green line) exhibits a more rapid decline in the number of objects (greater than 1 cm in size) over time, primarily due to enhanced atmospheric drag. The results of the simulation are normalised with respect to the initial number of generated fragments. The characteristics of the fragmentation are reported in Table 2.

It is therefore necessary to take into account several aspects that could lead to different consequences, in case of fragmentation, on the environment around the Earth.

This work attempts to investigate of in-orbit fragmentation using the space capacity concept, which is still in its early stages with new models being proposed in recent years. These models aim to define a sustainable threshold

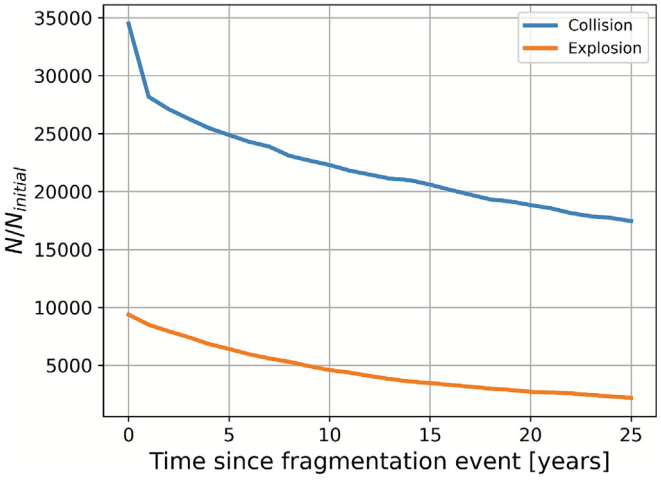

Fig. 1. Temporal evolution of the fragment population resulting from a catastrophic collision (blue) compared with that from an explosion event (orange). (For interpretation of the references to colour in this figure legend, the reader is referred to the web version of this article.)

Table 1
Collision versus explosion - fragmentation characteristics.

Event type	Altitude [km]	Inclination [deg]	Mass [kg]
Collision	855.00	98.64	950
Explosion	855.00	98.64	950

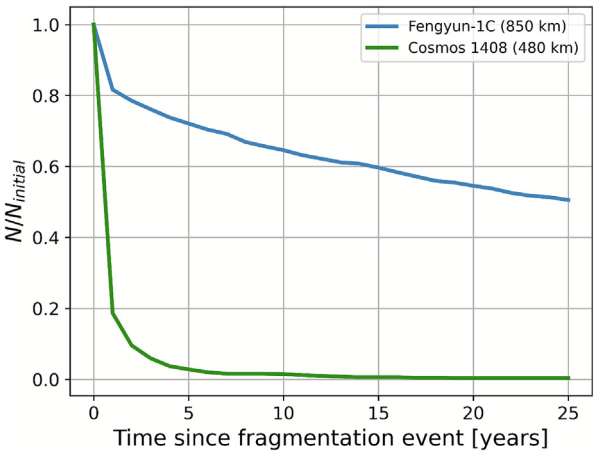

Fig. 2. Temporal evolution of the fragment population for events occurring at higher (blue) and lower (green) altitudes, with values normalised to the initial fragment count at the time of breakup. (For interpretation of the references to colour in this figure legend, the reader is referred to the web version of this article.)

Table 2
Location - fragmentation characteristics.

Event type	Altitude [km]	Inclination [deg]	Mass [kg]
Collision	850.00	98.64	950
Collision (hyper-velocity impact)	480.00	83.00	950

that the space environment can carry, in other words, a threshold that can still guarantee safe launches and satellite operations in the future, and to link those measures to the contribution of each new and already flying objects to it (i.e. the share of each object) which can also be seen as the portion of capacity consumed by the individual objects. This definition should then be shared and recognised internationally so that guidelines for launches, debris mitigation, and, more generally, global Space Traffic Management can be established. In general, some models attempt to define a space capacity by determining the maximum number of satellites that can be safely maintained in orbit (D'Ambrosio and Linares, 2024), while others attempt to define a space capacity by using a risk metric as the basis of the model (Krag et al., 2017; Letizia et al., 2020; McKnight et al., 2024a; Lewis and Marsh, 2021; Wang et al., 2024).

The concept of space capacity is therefore useful, as the introduction of debris resulting from a fragmentation event will interact with other orbiting objects around the Earth. This interaction may lead to the inaccessibility of some orbital regions, thereby reducing the overall availability of space for future launches, hence contributing to the consumption of the overall space capacity.

The paper is organised as follows. Section 2 describes the space capacity model adopted in this work. Section 3 presents the model that has been defined to integrate the study of fragmentations with that of space capacity. Section 4 analyses the results of some test cases comparing the results of several fragmentation events, simulated in different locations and with a different amount of mass involved. Section 5 concludes the work and includes possible future developments.

2. Space environmental impact and capacity definition

The definition of the space capacity model used in this work is based on the use of a risk metric (to assess the impact of single missions on the space environment), considering the results as the share of capacity used by that mission. This section briefly introduces the main ingredients of the metric, while a more detailed description can be found in Letizia et al. (2016), Colombo et al. (2023b), and Muciaccia et al. (2025b).

At each epoch of the mission, the Environmental Impact (EI) is evaluated as

$$I = p_c \cdot e_c + p_e \cdot e_e \tag{1}$$

where p_c and p_e denote the probabilities of collision and explosion, respectively, and e_c and e_e represent the corresponding severities of collision and explosion (Giudici et al., 2024; Giudici et al., 2023). The results are then aggregated over the entire mission to obtain the impact of the mission

$$EI = \int_{t_0}^{t_{EOL}} I\,dt + \alpha \int_{t_{EOL}}^{t_{end}} I\,dt + (1-\alpha) \int_{t_{EOL}}^{t_f} I\,dt \tag{2}$$

where t_0 is the starting epoch, and t_{EOL} is the epoch marking the end of the operational phase. The first term on the right-hand side of Eq. 2 corresponds to the operational phase of the object. The second and third terms refer to the Post Mission Disposal (PMD) phase, incorporating the potential failure of the End-Of-Life (EOL) disposal process (Letizia et al., 2019). Furthermore, the reliability of the PMD is accounted for through the parameter α (ranging from 0 to 1). Here, t_{end} denotes the epoch at which the disposal concludes, and t_f is the epoch at which the object would naturally re-enter from its initial orbit. An upper bound can be imposed on t_f, for example, 100 years (Letizia et al., 2019).

The space capacity *consumed* by a defined population of orbiting objects is instead quantified through the aggregation of the Environmental Impact (EI) metrics associated with each individual mission (Colombo et al., 2023a; McKnight et al., 2024a)

$$C = \sum_{j=1}^{N_m} EI_j \tag{3}$$

where EI_j is the environmental impact of the $j-th$ object considered in the set, and N_m is the total number of objects (either active or inactive) considered in the analysis. This type of definition, as opposed to just calculating the number of objects, introduces a perspective that also considers the possible consequences of fragmentations and their interaction with other orbiting objects. It is important to note that the capacity model used in this work is one of the space capacity models currently under development and being compared against each other (Letizia et al., 2024; McKnight et al., 2024b; Muciaccia et al., 2025a; Giudici and Neri, 2025). Nevertheless, the general framework for assessing the level of risk of in orbit fragmentation has been developed to work with different space capacity models, should that be necessary.

3. Evaluation model

The developed model aims to understand the possibility of using a space capacity model to level the risk of in-orbit fragmentation events. To do so, the workflow depicted in Fig. 3 is considered. Similar approaches have been proposed in the literature, where previous studies have attempted to analyse the problem, resulting in the development of analytical indices to rank fragmentation events and assess the severity of their environmental impact (Rossi et al., 2016; Rossi et al., 2015).

The proposed model is based on the comparison of two distinct scenarios. In the first, the temporal evolution of a reference population of orbiting objects is assessed under nominal conditions. In the second, the same population is analysed, but with the introduction of a fragmentation event. This comparative approach enables the evaluation of the impact of the fragmentation by highlighting differences in the population's evolution with and without the additional fragments. The generated debris interact with the original population, potentially altering its long-term dynamical behaviour and environmental sustainability.

The scenario, as in general the environment's long-term propagation, is mainly defined in terms of:

- Initial population: population of active and inactive objects, together with the background population;
- Launch traffic: pattern being considered for future launches;
- PMD strategy: the way, or at least the time, in which orbiting objects will be disposed of.

The fragmentation event is defined by key parameters, including the event type (e.g., collision or explosion), the

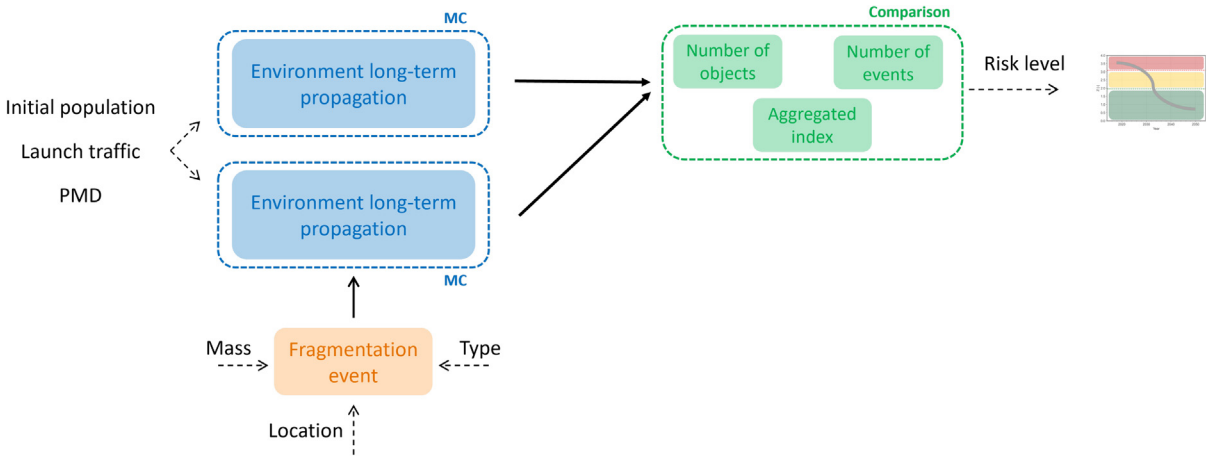

Fig. 3. Risk level evaluation - model workflow.

mass of the objects involved, and the orbital configuration (in terms of orbit altitude and inclination).

Downstream of propagation, several properties of the evolution of the environment are available. First, the number and properties (e.g., Keplerian elements and physical characteristics of each individual object) of the different orbiting objects (at different snapshot epochs), whose information can be used to understand how many uncontrollable objects (i.e., space debris) have been introduced into the population. This trend is related to the fragmentation events that occurred during propagation, which is also the second piece of information that can be extracted from the simulation results. Based on the evolution of these two pieces of information, it is possible to understand how stable or unstable the initial population and boundary conditions (such as PMD) are for a sustainable evolution of the space. However, counting only the number of objects and fragmentation events is not enough to understand the level of risk a fragmentation poses to the environment, while understanding how the fragments interact with the rest of the objects and how this leads to a space that can still be used is crucial. Thus, in addition to the other results, information on the capacity consumed (following Section 2) at different epochs of the propagation is obtained. Finally, a metric is introduced to investigate the difference between the two evolutionary trends in terms of space capacity, expecting similar behaviour in the case where fragmentation is not dangerous or different behaviour in the case where fragmentation is dangerous.

The nature of the available output data guided the selection of metrics. Specifically, the temporal evolution of both the reference scenario and the fragmentation scenario is simulated multiple times using a Monte Carlo (MC) approach to enhance the statistical robustness of the analysis. This is because the evolutionary model considered is ESA DELTA 4 (Bastida Virgili, 2016), which is semi-deterministic. Consequently, this implies multiple simulations of the same scenario, producing a distribution of outcomes (including the evaluated capacity at various snapshot epochs). The metric for the comparison of the two scenarios is hence based on the investigation of the distribution in terms of the consumed capacity of the two cases to understand *if* and *how much* the two behaviours differ from each other. Moreover, the score can be used in two distinct ways: firstly, to assign a risk level to a fragmentation event; and secondly, to analyse its temporal evolution in order to determine *if* and *when* it realigns with the reference scenario.

In this view, two approaches were considered: the first assumes normally distributed data (see Section 3.1), while the second assumes non-normally distributed data (see Section 3.2). As stated, the former requires normal distributions to work; consequently, the capacity samples were investigated to check whether they belonged to a normal distribution (A). However, it is important to note that, in general, evolutionary models do not exhibit normal (i.e., Gaussian) behaviour (Lidtke et al., 2017). Because of this, the second metric, which is based on generally distributed data, was introduced.

In both cases, the score obtained from the computation is compared to some defined limits coming from the literature to assign a level of risk to the fragmentation and evaluate for how long the risk level remains. For simplicity, three risk ranges were initially considered: low, medium and high.

The selection of metrics began with simple choices that nevertheless provided reliable, interpretable results. Overall, the focus was on choosing metrics that would highlight differences between the two distributions (and how large those differences were), with particular emphasis on their average behaviour. Anyway, the current model is flexible enough to allow the metric to be changed in future.

In the following subsections, the score metrics will be described in detail.

3.1. Normally distributed data

The first metric is based on the one-tailed Z-test (typically used to compare two normal distributions), considering the following null and alternative hypotheses

$$\begin{cases} H_0 : C_{frag} = C_{ref} \\ H_1 : C_{frag} > C_{ref} \end{cases} \tag{4}$$

with C_{frag} describing the distribution of the capacity for the fragmentation scenario, while C_{ref} is the distribution of the reference scenario, both evaluated at a specific snapshot scenario. The alternative hypothesis is defined using only the ">" operator, as the objective of the investigation is to determine whether (and to what extent) the capacity level increases when the fragmentation event is introduced.

The Z-score is computed at each epoch y as follows (Hogg and Tanis, 2015)

$$Z_y = \frac{\overline{C}_{frag_y} - \overline{C}_{ref_y}}{\sqrt{\sigma^2_{C_{frag_y}} + \sigma^2_{C_{ref_y}}}} \tag{5}$$

where $\overline{C}_{\mathrm{frag}_y}$ represents the mean value of the fragmentation scenario at the y-th epoch, $\overline{C}_{\mathrm{ref}_y}$ denotes the mean value of the reference scenario at the same epoch, and $\sigma^2_{C_{\mathrm{frag}_y}}$ and $\sigma^2_{C_{\mathrm{ref}_y}}$ correspond to the variances of the respective means, computed as the standard deviation divided by the square root of the number of MC simulations considered.

Then, three risk levels, according to statistics, are defined as shown in Fig. 4. A score exceeding 3.1 (Foll and Gaggiotti, 2008) indicates that the evolution of the environment differs significantly from the reference scenario, whereas a score below 1.96 (Hogg and Tanis, 2015; Montgomery and Runger, 2010) suggests that the two behaviours can be considered statistically similar.

3.2. Generally distributed data

The second metric is based on the Mann–Whitney U test (Mann and Whitney, 1947; Romano and Kromrey, 2006), used to compare non-normal distributions with small sample size, considering the same null and alternative hypotheses of the previous case (Eq. 4). Differently from before, this test cannot be used directly to quantify the level of differences in the two scenarios, but only to see if there is a significant difference. Then, the test is coupled with a metric, the Rank-Biserial Correlation (RBC) (Kerby, 2014; Cohen, 1988), typically used to compare two independent groups when the data is non-normally distributed. The metric is defined as

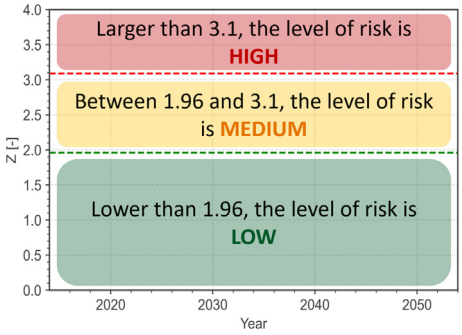

Fig. 4. Classification of risk level according to the Z-score.

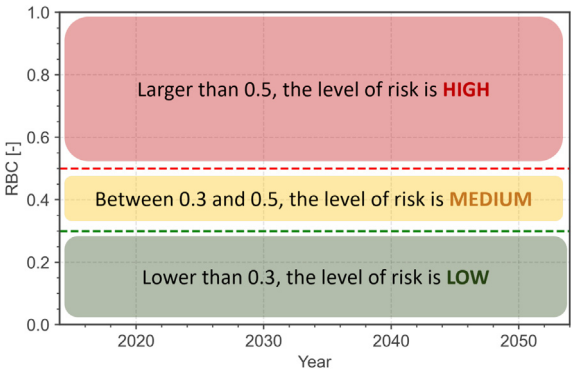

Fig. 5. Classification of risk level according to the Rank-Biserial Correlation.

$$RBC_y = 1 - \frac{2U_y}{N_1 N_2} \tag{6}$$

where U_y is the Mann–Whitney U statistic, N_1 and N_2 are the sample sizes of groups 1 and 2, respectively. Moreover, the RBC values range from -1 to 1, with positive values indicating that $C_{frag} > C_{ref}$.

As before, three risk levels, according to statistics, are defined as shown in Fig. 5. Whenever the score exceeds 0.5, the environmental evolution is considered to differ substantially from the reference scenario, whereas a score below 0.3 indicates that the two behaviours can be regarded as similar (Cohen, 1988).

4. Fragmentation events investigation

The reference scenario adopted in this study is based on the population of orbiting objects as of 1st January 2014 (Letizia et al., 2023), as available in ESA's DISCOS database. Starting from this original population, the future population is generated using a repeated launch traffic every 5 years, considering historical data from 2009 to 2014 available in the ESA DISCOS database (including data not publicly available) and discarding satellite constellations (still considering any objects already launched but as single spacecraft). The model considered keeps the number of active objects in orbit stable, considering the new objects launched and those re-entering. The latter happens after a lifetime of 8 year for each active spacecraft. In addition, the collision avoidance capabilities are disabled, an assumption already considered in past works (Rossi et al., 2016) when dealing with long-term propagations to reduce computational cost while keeping the result consistent with the aim of the study.

Regarding the type of fragmentation events that may occur during the propagation, collision events are considered, discarding possible explosion events (assumption considered also in past works Rossi et al. (2016)). This hypothesis is introduced to investigate the impact of

collision events, only. Indeed, only the collision part of the EI metric in 1 will be considered to compute the consumed capacity.

Fig. 6 illustrates the temporal evolution of the number of objects larger than 10 cm in the reference scenario. The dark line represents the mean value, while the lighter lines indicate the lower and upper bounds derived from the simulation results. The scenario is propagated for 200 years into the future using the ESA DELTA4 Bastida Virgili (2016) evolutionary model and by running 40 MC simulations (computational limits of internal server facility). At the beginning of the simulation, the population of objects larger than 10 cm consisted of: 17.5% of payloads (active and inactive), 7% of rocket bodies, and 75.5% of debris. As expected, the number of objects is increasing because of fragmentation events occurring in the simulations.

4.1. Fragmentation test cases

Multiple fragmentation events are considered to validate the proposed model. The test cases involve catastrophic collisions occurring on orbits with varying altitudes and inclinations and with varying fragment masses. In addition, in all test cases, the fragmentation has been introduced at the beginning of the simulation to simplify the process. However, the model can also introduce fragmentation at other epochs of the simulation and is not constrained to the initial epoch.

Furthermore, based on the results obtained and prior studies (Rossi et al., 2016), the analysis focuses primarily on the evaluation of capacity during the initial years following the fragmentation event, although data extending further in time are also available. As illustrated, for example, in Fig. 7, the divergence between the fragmentation scenario and the baseline scenario is typically more pronounced in the period immediately following the event than at later times. Unlike the reference scenario, for both fragmentation scenarios (blue and red lines), only the MC mean value is shown; the same convention is used in all the figures of this paper for both the population and the space capacity evolutions.

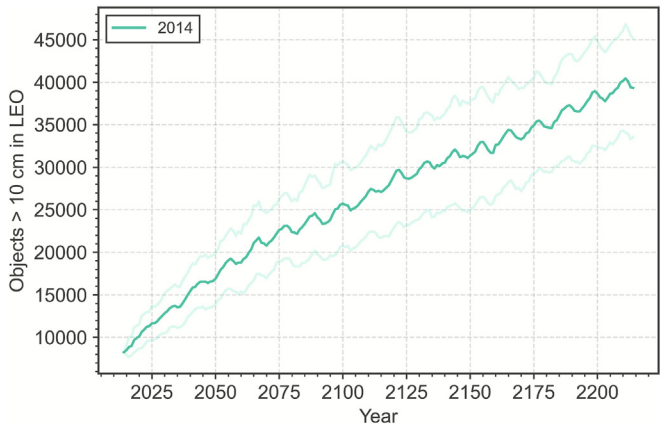

Fig. 6. Temporal evolution of the number of objects larger than 10 cm in LEO - Reference scenario.

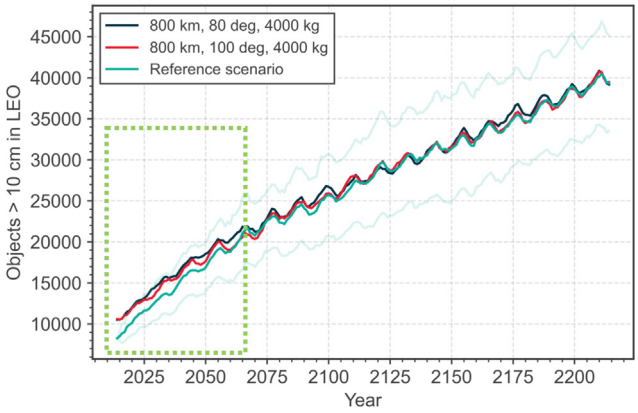

Fig. 7. Temporal evolution of the number of objects larger than 10 cm, comparing two fragmentation events occurring at the same altitude but with different inclinations - LEO.

4.1.1. Fragmentation location

The locations of the investigated fragmentations were not randomly selected, but maps showing the severity of a fragmentation were used as a starting point. Indeed, these maps provide insight into which regions would have a greater impact on the population of active objects in the event of a fragmentation, mainly from a cumulative collision risk perspective (see B for more detail).

Three orbital configurations (defined by orbit altitude and inclination) have been considered, with four possible involved masses. Two at low altitude (around 800 km) and one at high altitude (around 1600 km). The study parameters are summarised in Table 3, while the fragmentation locations are shown in Fig. 8. The three selected orbital slots correspond to: 800 km at 80°, where the severity map shows its maximum, representing the region with the highest potential impact on the active population in the event of a fragmentation; 800 km at 100°, corresponding to the highest concentration of active orbiting objects in 2014; and 1,600 km at 80°, representing a region with a very low density of objects.

4.1.2. Evolution of space capacity following fragmentation at various orbital altitudes and inclinations

. As stated in the previous section, three orbital configurations (defined by altitude and inclination) are considered for the fragmentation events. In this first case, a fragmentation involving a mass of 4000 kg is simulated at an altitude of 800 km: first at an inclination of 80°

Table 3
Fragmentation events characteristics.

(Altitude [km],Inclination [deg])	(800,80), (800,100), (1600,80)
Mass [kg]	500, 1000, 4000, 8000

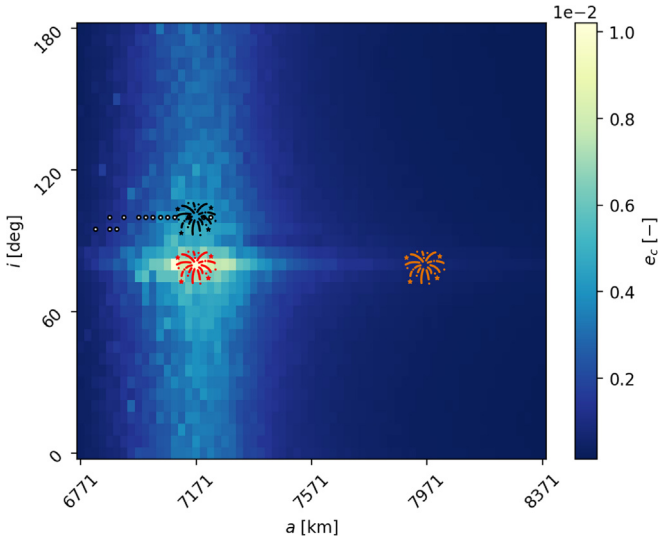

Fig. 8. Catastrophic collision effect maps computed based on target populations as of 1st January 2014 - black, red, and orange fireworks icons show the semi-major axis and inclination of the fragmentation orbit. (For interpretation of the references to colour in this figure legend, the reader is referred to the web version of this article.)

(corresponding to the peak in the severity map shown in Fig. 8), and then at 100°. Before analysing the evolution of capacity associated with these scenarios, it is interesting to examine the temporal evolution of the number of objects throughout the simulation and to assess the differences in spatial density between the fragmentation and reference scenarios. This is illustrated in Fig. 7, where it can be observed that, following an initial divergence, the trends gradually converge towards the reference scenario. This behaviour can be attributed to the re-entry of a portion of the fragments at this altitude, as well as to the DELTA 4 model, which simulates additional collision events every year based on a stochastic method (Bastida Virgili, 2016), thereby contributing to a progressive increase in the overall object population. The same phenomena can be observed by looking at the plots of the spatial density, at the beginning of the simulation (Fig. 9a) and the year 2074 (Fig. 9b).

In the beginning, there is a big difference in the distribution around the fragmentation altitude. This difference tends to diminish as more fragmentations are simulated in the propagation.

With this in mind, the temporal evolution of space capacity shown in Fig. 10 (which only reports the average values of MCs) reveals that, initially, both fragmentation scenarios exhibit higher capacity consumption compared to the reference. However, over time, the values converge towards the reference scenario. This indicates that, following an initial period of divergence, the consumed capacity level returns to that of the baseline scenario.

A third simulated fragmentation event considered a mass of 8000 kg, occurring at an altitude of 1600 km and an inclination of 80°. The evolution of the number of objects larger than 10 cm is presented in Fig. 11. As shown, when the fragmentation occurs at a higher altitude, the resulting fragments take longer to re-enter the atmosphere. This may be the reason why the trend remains above that of the reference scenario. In addition, Fig. 12 shows the spatial density at the beginning of the simulation. As before, the main difference is around the position of fragmentation.

4.1.3. Z-score

The difference between the fragmentation scenarios and the reference scenario is investigated by applying the model introduced in Section 3, considering the data as normally distributed.

First, the fragmentations at a lower altitude are considered (i.e., Fig. 7). As shown in Fig. 13, both scenarios fall within the 'high' risk category, with similar Z-score values. Contrary to what one might infer looking at the effect maps (Fig. 8), there is no greater effect for the fragmentation on an 80° orbit. Indeed, a breakup at 80° places the fragments in a geometry that is more hazardous relative to the majority of operational satellites (particularly sun-synchronous spacecraft at 100°) in terms of both collision probability and potential severity. The impact rate between fragments and a potential target is influenced by their relative

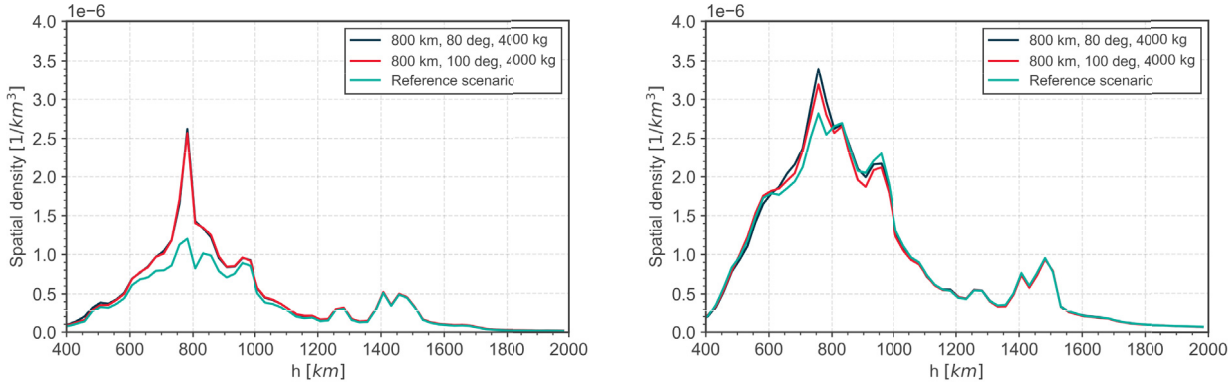

(a) Year 2014.

(b) Year 2074.

Fig. 9. Spatial density of the fragmentation scenarios and reference scenario at the beginning of the simulation (left) and the year 2074 (right).

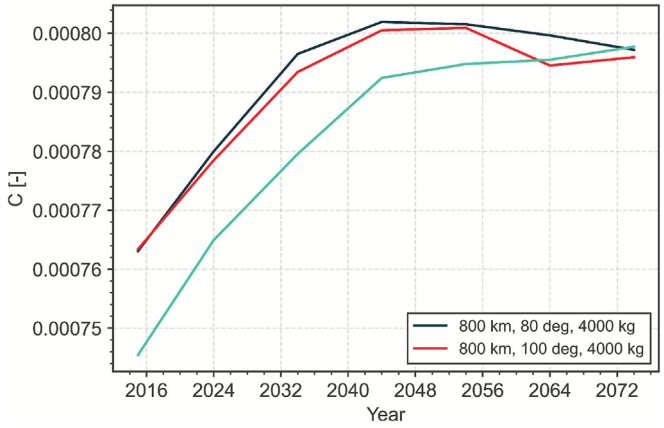

Fig. 10. Evolution of consumed space capacity over time (mean value across all MC runs) for fragmentation events at the same altitude but different inclinations.

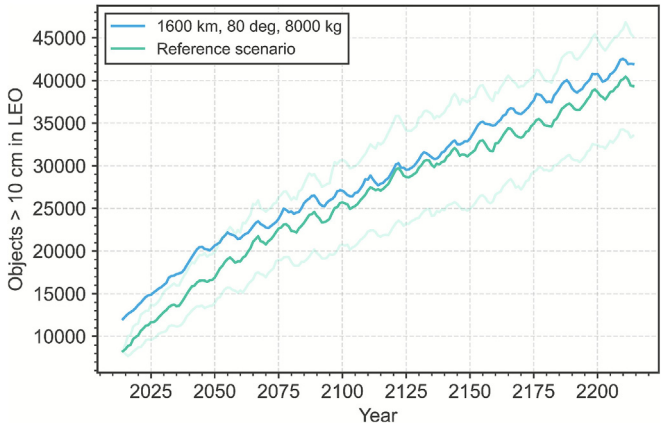

Fig. 11. Temporal evolution of the number of objects larger than 10 cm following a high-altitude fragmentation event in LEO.

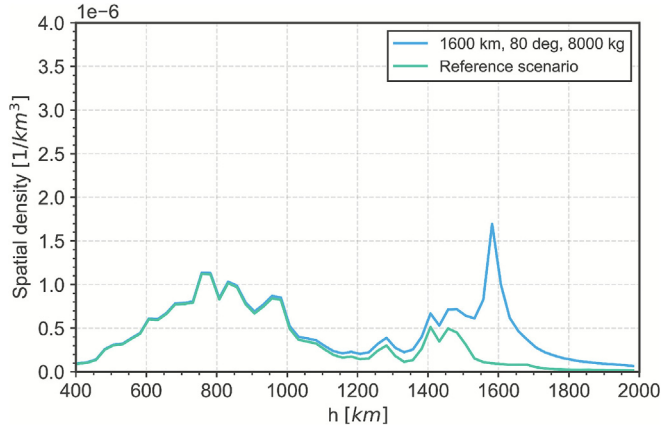

Fig. 12. Spatial density of the fragmentation and reference scenarios at the beginning of the simulation - high altitude case.

velocity, which is maximised when their orbital configurations are symmetric about 90° inclination (Giudici et al., 2024). This is a result that could also be appreciated by

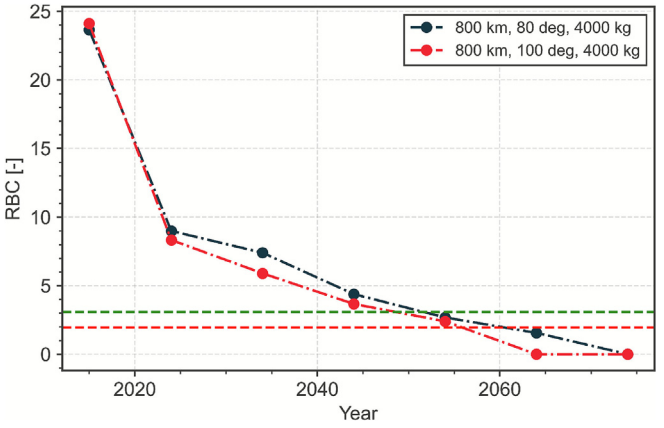

Fig. 13. Z-score evolution over time - same altitude, different inclination.

looking at the severity map (Fig. 8), where the peak in terms of severity of fragmentation is at 800 km altitude and 80° in inclination.

Thanks to the consumed capacity definition considered, it is also possible to do further analysis by dividing LEO into two height sub-regions: low height up to 1200 km (yellow) and high height above 1200 km (brown). The consumed capacity is then calculated in these two regions. This is because, as can be seen from the Fig. 14a, the debris generated by the fragmentation mainly changes the region at low altitudes, leaving the region at high altitudes almost unchanged. Consequently, as can be seen from Fig. 14b, the level of risk is ”high” for the low altitude region, while ”low” for the high altitude region. This application shows how the versatility of the definition also allows to focus on sub-regions of interest.

The evolution of the Z-score associated with the fragmentation at 1600 km is shown in Fig. 15. In this third case, the fragmentation is classified as posing a ”low” risk. This is because the resulting fragments do not significantly intersect high-risk regions populated by operational satellites, and therefore have a limited impact on overall collision probability.

4.1.4. RBC-score

The difference between the fragmentation scenarios and the reference scenario is again investigated by applying the model introduced in Section 3, but considering the data as non-normally distributed.

Again, regarding the fragmentations at a lower altitude, both scenarios fall into the level of risk ”high”, as shown in Fig. 16. As before, the case at a lower inclination (dark blue) has the same initial value as the case at a higher inclination (red) but tends more slowly toward the baseline.

4.1.5. Fragmentation with different masses

In the second set of test cases, the location of the fragmentation is considered fixed (i.e., at an altitude of 800 km and with an inclination of 80°) but the mass involved changes (Table 3). The evolution of the number

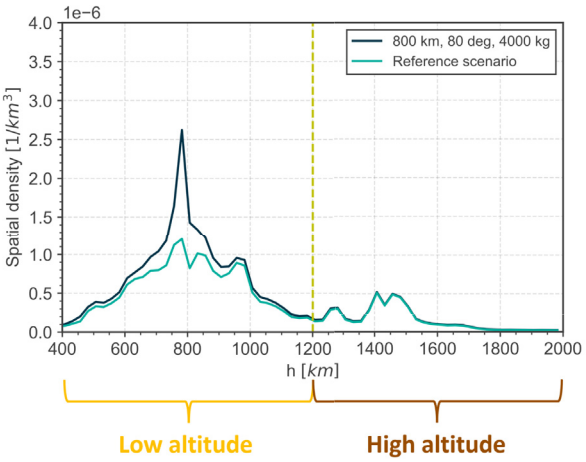

(a) Spatial density at 2014.

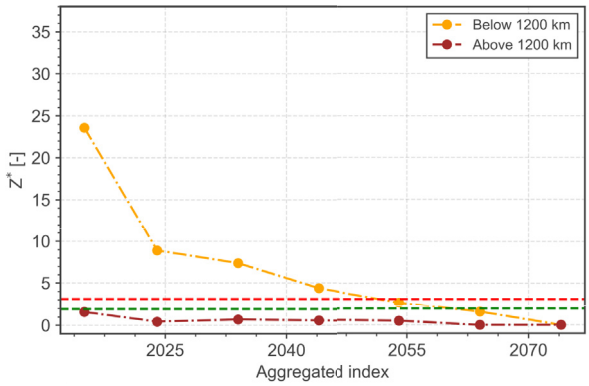

(b) Z-score evolution of the low altitude (yellow) and high altitude (brown) cases over time.

Fig. 14. Comparison between low altitude (yellow) and high altitude (brown). (For interpretation of the references to colour in this figure legend, the reader is referred to the web version of this article.)

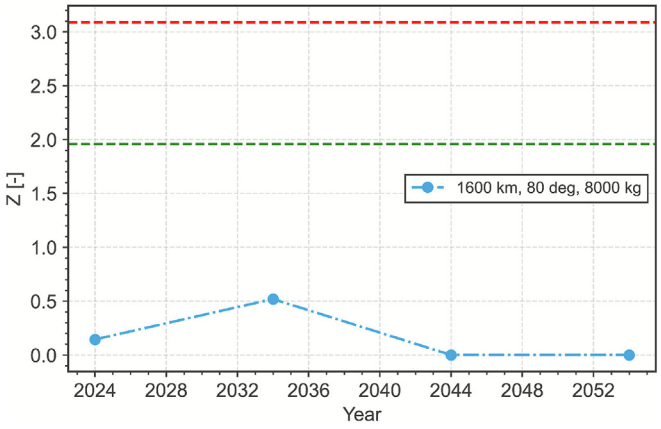

Fig. 15. Z-score evolution over time - higher altitude.

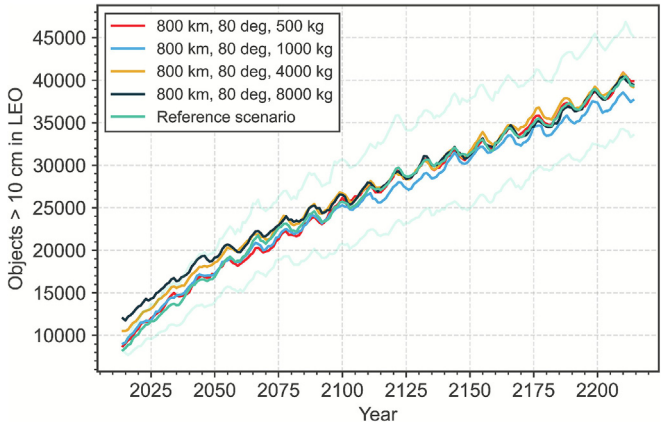

Fig. 17. Temporal evolution of the number of objects larger than 10 cm, considering fragmentation events involving different masses - LEO.

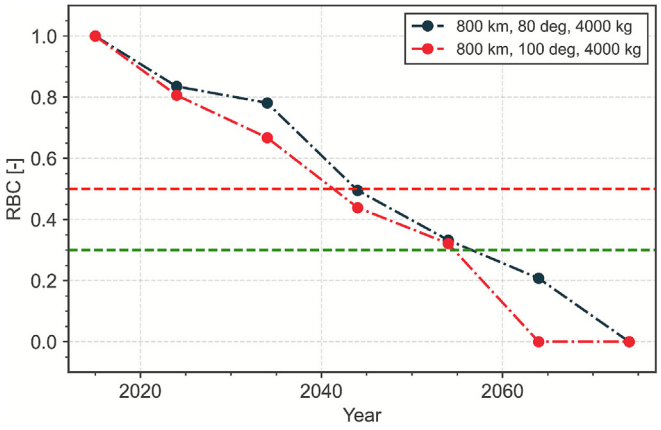

Fig. 16. RBC-score evolution over time - same altitude, different inclination.

of objects (Fig. 17) and and the spatial density (Fig. 18) shows that, as expected, the more the mass increases, the more there is a difference with the reference scenario. In all the cases, however, the trend tends to that of the reference scenario. The speed at which this happens is inversely proportional to the mass; this probably occurs because the other fragmentations simulated by the DELTA 4 model introduce enough debris to make the impact of that single fragmentation less significant.

Fig. 19 presents the temporal evolution of space capacity for each simulated fragmentation scenario. A common feature across all the test cases is the initial increase in the capacity consumed, followed by a gradual convergence towards the capacity level of the reference scenario. In particular, the reference scenario is the only one exhibiting a continuous increase over time. This behaviour is similar to the evolution of the number of objects: an initially larger

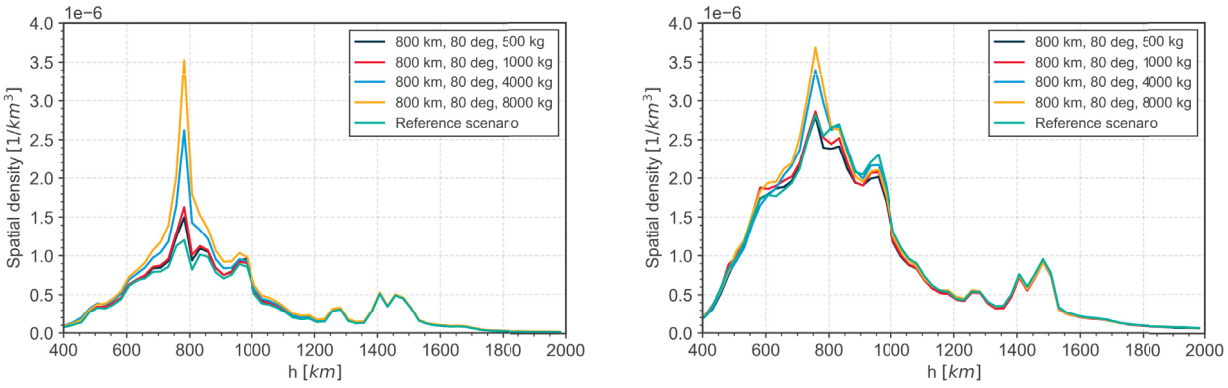

(a) Year 2014. (b) Year 2074.

Fig. 18. Spatial density of the fragmentation scenarios and reference scenario at the beginning of the simulation (left) and the year 2074 (right).

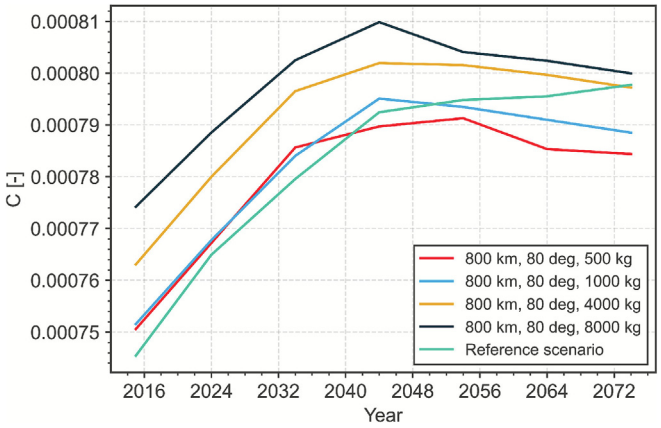

Fig. 19. Temporal evolution of space capacity (mean value across all MC simulations) - different masses.

population in the case of a fragmentation that gradually approaches the reference level. As a result, the background population becomes increasingly similar across scenarios (as illustrated in Fig. 18), leading to a convergence in collision probability.

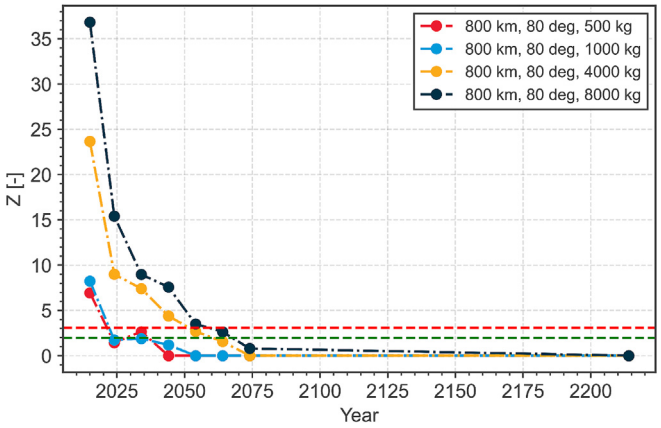

Fig. 20. Z-score evolution over time - different masses.

The Z-score is applied to all the test cases, and the results are shown in Fig. 20. As expected, by decreasing the mass the level of risk decreases (still remaining "high") and it is reabsorbed faster by the space environment.

5. Conclusion

The study of in-orbit fragmentations represents an important aspect of the broader topic of space sustainability. This work describes the model developed to assess the level of risk posed by in-orbit fragmentation on the space environment. The concept of consumed capacity (defined using a risk metric as a basis) provides a different perspective than simply studying the long-term evolution and computing the temporal evolution of the number of objects.

The model compares two scenarios, propagated into the future using debris evolutionary models, in terms of the evolution of consumed capacity, calculating how different the two trends are to see whether the impact is great or not. The level of difference is estimated in two ways:

- Z-score, assuming that the data are normally distributed;
- Mann–Whitney U test with the Rank-Biserial Correlation, assuming that the data are non-normally distributed.

To test the model, a reference scenario was defined considering the population in 2014, and several fragmentations were simulated, changing either the location or the mass involved in the event. The results showed that both the mass and the location, mainly in terms of orbit altitude and inclination, play a role in the level of risk posed by the fragmentation.

However, the investigation is still ongoing both to improve the model and to investigate new scenarios. Indeed, the original objective was to understand the feasibility of using the concept of capacity applied to in-orbit fragmentation. The next step would be to properly define the metric and risk levels that will be assigned to the

fragmentation events. The latter can be done by applying the model to a series of different events, modifying the type, the mass, and the geometry of the involved objects. Moreover, additional effects of fragmentation can be investigated, such as chain effects of the fragments generated by the investigated fragmentation and possible future breakup events.

Another interesting test that could be done is to apply the model to real-world scenarios, that is, to past fragmentation, to understand how much it actually impacted the environment. This can be done by extrapolating the population data at the time of the fragmentation, then adding fragmentation and comparing trends.

Declaration of competing interest

The authors declare that they have no known competing financial interests or personal relationships that could have appeared to influence the work reported in this paper.

Acknowledgments

This research has received funding from the European Research Council (ERC) under the European Union's Horizon Europe research and innovation programs, which are part of the GREEN SPECIES project (Grant Agreement No.101089265).

Appendix A. This section presents the tests performed to check the normality of the capacity distribution.

Due to computing resources, only 40 MC simulations were considered for each test case. The test was performed considering the Shapiro–Wilk test (Shapiro and Wilk, 1965), typically used to test the null hypothesis that the data was drawn from a normal distribution. The result is the p-value for the hypothesis test which, for samples taken from a normal distribution, gives a result greater than 0.05.

Table A.4 summarises the test outcome for the long-term propagation cases analysed in Section 4, looking at the capacity distributions.

Appendix B. This section provides an introduction to the computation of the severity maps (Fig. 8) and, consequently, to the interpretation of the severity term e of the Environmental Impact metric.

Starling 2.1 tool (Giudici et al., 2023) is used to generate these maps; the tool can simulate on-orbit fragmentations, model them, propagate the debris distribution using a continuous model (Giudici et al., 2023), and assess the collision probability (Giudici et al., 2024) of the fragments with other orbiting objects.

The map is generated in two steps: first, selecting the target objects on which the cumulative collision probability will be computed; second, generating dummy fragmentations, propagating them, and assessing their effect on the selected targets. Both steps are carried out using a grid in Keplerian orbital elements, specifically semi-major axis and inclination for LEO objects. Within the grid, a target is defined for any bin in which the cumulative cross-sectional area of all the objects in the bin exceeds a specified threshold (25 km in this work) (Muciaccia et al., 2025b). The generated target is characterised by the average physical properties of all objects in that bin. Then, the severity of each fragmentation event, evaluated on the same grid, is assessed in three main steps:

- Determination of the initial fragment density distribution by means of a probabilistic reformulation of the NASA Standard Breakup Model (SBM) (Giudici et al., 2023; Frey and Colombo, 2021)
- Propagation of the fragment density using the method of characteristics (Johnson et al., 1981), followed by interpolation of the characteristics via binning in the 7-D phase space of Keplerian elements and area-to-mass ratio (Giudici et al., 2023)
- Assessing the cumulative number of impacts on each target within the considered time window (Giudici et al., 2024).

After performing these steps, the severity of each fragmentation is evaluated according to the following metric:

Table A.4
P-value from the Shapiro–Wilk test for each long-term propagation scenario.

Scenario	2015	2024	2034	2044	2054	2064	2074
Reference	0.137	0.880	0.151	0.348	0.674	0.736	0.583
800 km 80 deg 500 kg	0.373	0.266	0.414	0.485	0.163	0.159	0.562
800 km 80 deg 1000 kg	0.452	0.509	0.217	0.545	0.517	0.426	0.841
800 km 80 deg 4000 kg	0.442	0.265	0.880	0.106	0.647	0.412	0.860
800 km 80 deg 8000 kg	0.091	0.530	0.248	0.836	0.496	0.008	0.884
800 km 100 deg 500 kg	0.395	0.315	0.925	0.073	0.907	0.779	0.149
800 km 100 deg 1000 kg	0.431	0.271	0.752	0.281	0.256	0.575	0.744
800 km 100 deg 4000 kg	0.411	0.293	0.625	0.218	0.851	0.540	0.382
800 km 100 deg 8000 kg	0.590	0.123	0.761	0.080	0.783	0.373	0.634
1600 km 80 deg 8000 kg	-	0.486	0.647	0.132	0.341	-	-

$$e(\Delta t) = \frac{\sum_{i=1}^{N_t} P_{c_i}(\Delta t) \cdot A_{t_i}}{A_{tot_0}} \tag{B.1}$$

where

$$P_{c_i}(\Delta t) = 1 - e^{-\phi \cdot A_i \cdot \Delta t} \tag{B.2}$$

with ϕ the debris flux in $1/\text{km}^2/\text{year}$, A_i is the average area in the $i-th$ bin, Δt is the time considered in year (15 years for this work), A_{t_i} is the total cross-sectional area of the $i-th$ bin, and A_{tot} is the cumulative cross-sectional area in the bins hosting a target at a reference epoch.

An example of a map generated by this procedure is Fig. 8, which shows the severity map obtained by selecting targets from the population of active orbiting objects in 2014. The map indicates that, in lighter regions, a fragmentation would have a high severity for the selected targets, whereas in darker regions its impact would be smaller.

References

Bastida Virgili, B., 2016. Delta (debris environment long-term analysis). In: 6th International Conference on Astrodynamics Tools and Techniques (ICATT), Darmstadt, Germany.

Cohen, J., 1988. Statistical Power Analysis for the Behavioral Sciences, 2nd ed. Routledge, New York.

Colombo, C., Giudici, L., Muciaccia, A. et al., 2023a. Assessment of the collision risk in orbital slots and the overall space capacity. In: 2nd International Orbital Debris Conference, Sugar Land, Texas.

Colombo, C., Muciaccia, A., Giudici, L. et al., 2023b. Tracking the health of the space debris environment with themis. In: Joint 10th EUCASS - 9th CEAS Conference, Lausanne, Switzerland.

D'Ambrosio, A., Linares, R., 2024. Carrying capacity of low earth orbit computed using source-sink models. J. Spacecr. Rock. https://doi.org/10.2514/1.A35729.

ESA Space Debris Office, 2024. ESA's annual space environment report. Technical Report Technical report. https://www.sdo.esoc.esa.int/environment_report/Space_Environment_Report_latest.pdf.

Foll, M., Gaggiotti, O., 2008. A genome-scan method to identify selected loci appropriate for both dominant and codominant markers: a bayesian perspective. Genetics 180 (2), 977–993.

Frey, S., Colombo, C., 2021. Transformation of satellite breakup distribution for probabilistic orbital collision hazard analysis. J. Guid., Control, Dynam. 44 (1), 88–105. https://doi.org/10.2514/1.G004939.

Giudici, L., Gonzalo, J.L., Colombo, C., 2024. Density-based in-orbit collision risk model valid for any impact geometry. Acta Astronautica, 219, 785–803. URL: https://www.sciencedirect.com/science/article/pii/S0094576524001930. doi: 10.1016/j.actaastro.2024.03.067.

Giudici, L., Neri, M., 2025. Development of a software architecture for comparing existing orbital carrying capacity models. In: 9th European Conference on Space Debris, URL: https://conference.sdo.esoc.esa.int/proceedings/sdc9/paper/60.

Giudici, L., Trisolini, M., Colombo, C., 2023. Probabilistic multi-dimensional debris cloud propagation subject to non-linear dynamics. Adv. Space Res. 72 (2), 129–151. https://doi.org/10.1016/j.asr.2023.04.030.

Hogg, R.V., Tanis, M., 2015. Introduction to Mathematical Statistics, 7th ed. Pearson.

Johnson, N., Krisko, P., Liou, J.-C. et al., 2001. Nasa's new breakup model of evolve 4.0. Adv. Space Res., 28(9), 1377–1384. URL: https://www.sciencedirect.com/science/article/pii/S0273117701004239. doi: 10.1016/S0273-1177(01)00423-9.

Johnson, N.L., LaSalle, J.P., Sirovich, L., 1981. Partial Differential Equations. Springer.

Kerby, D., 2014. The simple difference formula: an approach to teaching nonparametric correlation. Comprehen. Psychol. 3. https://doi.org/10.2466/11.IT.3.1.

Kessler, D.J., Cour-Palais, B.G., 1978. Collision frequency of artificial satellites: the creation of a debris belt. J. Geophys. Res. 83 (A6), 2637–2646. https://doi.org/10.1029/JA083iA06p02637.

Krag, H., Lemmens, S., Letizia, F., 2017. Space traffic management through the control of the space environment's capacity. In: Proceedings of the 1st IAA Conference on Space Situational Awareness (ICSSA). Orlando, FL, USA.

Letizia, F., Bastida Virgili, B., Lemmens, S., 2023. Assessment of orbital capacity thresholds through long-term simulations of the debris environment. Advances in Space Research, 72(7), 2552–2569. URL: https://www.sciencedirect.com/science/article/pii/S0273117722004793. doi: 10.1016/j.asr.2022.06.010.

Letizia, F., Colombo, C., Lewis, H.G., et al., 2016. Assessment of breakup severity on operational satellites. Adv. Space Res. 58 (7), 1255–1274. https://doi.org/10.1016/j.asr.2016.05.036.

Letizia, F., Colombo, C., Rossi, A., et al., 2024. Mission-based and environment-based approaches for assessing the severity of a space debris evolution scenario from a sustainability perspective. In: 75th International Astronautical Congress (IAC).

Letizia, F., Lemmens, S., Bastida Virgili, B. et al., 2019. Application of a debris index for global evaluation of mitigation strategies. Acta Astronaut., 161, 348–362. URL: https://www.sciencedirect.com/science/article/pii/S009457651930222X. doi: 10.1016/j.actaastro.2019.05.003.

Letizia, F., Lemmens, S., Krag, H., 2020) Environment capacity as an early mission design driver. Acta Astronaut., 173, 320–332. URL: https://www.sciencedirect.com/science/article/pii/S0094576520302459. doi: 10.1016/j.actaastro.2020.04.041.

Lewis, H.G., Marsh, N., 2021. Deep time analysis of space debris and space sustainability. In: Proceedings of the 8th European Conference on Space Debris (Virtual).

Lidtke, A.A., Lewis, H.G., Armellin, R., 2017. Statistical analysis of the inherent variability in the results of evolutionary debris models. Adv. Space Res. 59 (7), 1698–1714. https://doi.org/10.1016/j.asr.2017.01.004.

Mann, H.B., Whitney, D.R., 1947. On a test of whether one of two random variables is stochastically larger than the other. Annals Math. Stat. 18 (1), 50–60. https://doi.org/10.1214/aoms/1177730491.

McKnight, D., Dale, E., Colombo, C. et al., 2024a. Normalizing orbital capacity characterization. In: Proceedings of the 75th International Astronautical Congress (IAC).

McKnight, D.F., Dale, E., Colombo, C. et al., 2024b. Normalizing orbital capacity characterization. In: 75th International Astronautical Congress (IAC).

Montgomery, D.C., Runger, G.C., 2010. Applied Statistics and Probability for Engineers, (5th ed.). John Wiley & Sons.

Muciaccia, A., Colombo, C., McKinght, D. et al., 2025a. Space capacity methodologies to rank the risk of orbital regions. In: 9th European Conference on Space Debris. URL: https://conference.sdo.esoc.esa.int/proceedings/sdc9/paper/223.

Muciaccia, A., Giudici, L., Letizia, F. et al., 2025b. Evaluating the environmental impact of space missions. Acta Astronaut., 236, 239–250. URL: https://www.sciencedirect.com/science/article/pii/S0094576525003765. doi: 10.1016/j.actaastro.2025.06.024.

Romano, J., Kromrey, J., 2006. Appropriate statistics for ordinal level data: Should we really be using t-test and cohen's d for evaluating group differences on the nsse and other surveys? Florida Association of Institutional Research.

Rossi, A., Lewis, H., Alessi, E.M. et al., 2015. Fragmentation Consequence Analysis for LEO and GEO Orbits, Version 1.0. Executive Summary, ESA/ESOC No. Technical Report 4000106534/12/F/MOS, July.

Rossi, A., Lewis, H., White, A., et al., 2016. Analysis of the consequences of fragmentations in low and geostationary orbits. Adv. Space Res. 57 (8), 1652–1663. https://doi.org/10.1016/j.asr.2015.05.035.

Shapiro, S.S., Wilk, M.B., 1965. An analysis of variance test for normality (complete samples). Biometrika 52 (3–4), 591–611. https://doi.org/10.1093/biomet/52.3-4.591.

Wang, Y., De Marchi, P., Vasile, M., 2024. A stochastic dynamic network model of the space environment. arXiv preprint arXiv:2411.03173v1.